

Article

# Numerical Investigation to the Effect of Suction-Induced Seepage on the Settlement in the Underwater Vacuum Preloading with Prefabricated Vertical Drains

Shu Lin <sup>1</sup>, Dengfeng Fu <sup>2,\*</sup> , Zefeng Zhou <sup>3</sup>, Yue Yan <sup>2</sup> and Shuwang Yan <sup>2</sup>

<sup>1</sup> School of Civil Engineering and Architecture, Hainan University, Haikou 570228, China; linshu@hainanu.edu.cn

<sup>2</sup> State Key Laboratory of Hydraulic Engineering Simulation and Safety, School of Civil Engineering, Tianjin University, Tianjin 300072, China; yue.yan@tju.edu.cn (Y.Y.); yanshuwang@tju.edu.cn (S.Y.)

<sup>3</sup> DNVGL Renewable Energy, Tuborg Parkvej 8, 2900 Hellerup, Denmark; zefeng.zhou@dnv.com

\* Correspondence: dengfeng\_fu@tju.edu.cn

**Abstract:** Vacuum preloading combined with prefabricated vertical drains (PVDs) has the potential to improve the soft sediments under water, however, its development is partly limited by the unclear understanding of the mechanism. This paper aims to extend the comprehension of the influential mechanism of overlapping water in the scenario of underwater vacuum preloading with PVDs. The systematic investigations were conducted by small strain finite element drained analyses, with the separated analysis schemes considering suction-induced consolidation, seepage and their combination. The development of settlement in the improved soil region and the evolution of seepage flow from the overlapping water through the non-improved soil region into improved zone are examined in terms of the build-up of excess pore pressure. Based on the results of numerical analyses, a theoretical approach was set out. It was capable to estimate the time-dependent non-uniform settlement along the improved soil surface in response to the combined effects of suction-induced consolidation and seepage. The difference of underwater and onshore vacuum preloading with PVDs is discussed with some practical implication and suggestion provided.

**Keywords:** vacuum preloading; prefabricated vertical drains; consolidation; seepage; non-uniform settlement; overlapping water



**Citation:** Lin, S.; Fu, D.; Zhou, Z.; Yan, Y.; Yan, S. Numerical Investigation to the Effect of Suction-Induced Seepage on the Settlement in the Underwater Vacuum Preloading with Prefabricated Vertical Drains. *J. Mar. Sci. Eng.* **2021**, *9*, 797. <https://doi.org/10.3390/jmse9080797>

Academic Editor: Carl T. Friedrichs

Received: 9 May 2021

Accepted: 21 July 2021

Published: 24 July 2021

**Publisher's Note:** MDPI stays neutral with regard to jurisdictional claims in published maps and institutional affiliations.



**Copyright:** © 2021 by the authors. Licensee MDPI, Basel, Switzerland. This article is an open access article distributed under the terms and conditions of the Creative Commons Attribution (CC BY) license (<https://creativecommons.org/licenses/by/4.0/>).

## 1. Introduction

The recent development of marine resources has increased the need for engineers to improve the soft sediments under water. It is expected to be applied prior to the construction of marine structures, such as offshore foundations, cofferdams, wharfs, etc., ensuring a desirable margin of safety against the design loadings during service.

Vacuum preloading combined with prefabricated vertical drains (PVDs) is now the commonly employed ground improvement technique suitable for soft deposits to accelerate the dissipation of pore pressure resulted in an earlier settlement and a gain in undrained shear strength [1–3]. In the intertidal areas, several successful engineering practices have shown their validity and economy in improving the submarine soil [4–7]. In the deeper water, attempts have been seldom reported except for the pilot test at the water depth of 10 m performed by [8]. Yet, the success has proved the feasibility of underwater vacuum preloading, and it would be more competent with the advance of vacuum process.

Much research related to the vacuum preloading or combined with PVDs have been conducted, with the focus on the drainage behavior in the soil region required to be improved. The responses of pore water pressure, settlement, lateral displacement, consolidation rate and etc., were of great concerns in the study, where many influence factors were considered and investigated. They included anisotropy of permeability [9–11], permeability degradation [11–16], discharge capacity of drain [17–21], well resistance [13,22,23],

drain spacing [12,24], large strain [3,25], and so forth. These provided the increasing comprehensions of vacuum preloading with PVDs mechanism, and facilitated its development in the underwater application.

Toward the problem of underwater vacuum preloading, the soil necessary to be treated was covered by a certain depth of water (i.e., overlapping water), which was the main difference between onshore and offshore vacuum preloading. The overlapping water was thought to be an additional preloading [25–28] for the improved soil region during underwater vacuum preloading. In fact, this additional loading can also be understood from another aspect. The existence of overlapping water allowed the suction head (or measured excess pore pressure) larger than 100 kPa, that is an atmosphere pressure, to be achieved in the underwater vacuum preloading [8], although it is dependence of the capacity of submerged pump to do more work as to overcome the seabed water pressure of overlapping water. However, the overlapping water not only acted as a beneficial factor to increase consolidation settlement and thus soil strength, but possibly led to some unexpected problems, such as inefficiency of consolidation and larger post-construction settlement [29]. It is because the high suction head potentially induced seepage flow from the overlapping water through the soil domain into the improved soil zone [25,26].

While the general process of underwater vacuum preloading with PVDs is well recognized, interpretation of its mechanism has not been addressed adequately. In particular, the combination of consolidation and seepage mechanisms due to the existence of overlapping water is still not well understood, such as the influential region, magnitude, and duration of seepage. Considering these, the aim of this study is therefore to investigate the influential mechanism of overlapping water and interpret the counteraction mechanism of consolidation and seepage in the scenario of underwater vacuum preloading with PVDs, and develop a method to predict the contribution (perhaps negative) of seepage on the consolidation settlement.

The organization of this paper is as follows. First, a suite of finite element (FE) drained analyses were implemented including three schemes of suction-induced consolidation, seepage, and their combination. The responses of both improved soil and non-improved subsoil were included. Throughout these three analyses scenarios, the evolution of settlement along the top surface of improved soil region with the build-up of excess pore pressure was examined and compared to explore the influential mechanism of seepage underwater vacuum preloading. Second, a method was proposed underlying the consolidation mechanism combined with seepage, to predict the settlement response through the entire duration of underwater vacuum preloading and through the entire improved soil region. Finally, this paper concluded with discussion of some practical implications and suggestions by the comparison of responses in different water depths or durations of applied vacuum.

## 2. Finite Element Modelling

The coupled small-strain FE analyses were carried out with the commercially available software ABAQUS (ver. 6.10, accessed on 10 January 2011) [30], since it is particularly well-suited to simulate the seepage and consolidation scenarios in the geotechnical field.

### 2.1. Model Description

The soil region necessary to be improved with a breadth-to-height ratio  $B/H$  was considered in the simulation of underwater vacuum preloading. In practice, a layer of impermeable membrane is equipped with a group of prefabricated vertical drains (PVDs) into the improved soil for a stable suction during the vacuum preloading process. To represent field condition, the improved soil region was first partitioned horizontally, yielding a very thin top layer with the thickness of  $0.1H$  prescribed to be weightless and impermeable. Then, the several vertical partitions were applied with the spacing ratio of  $b/B$  (here, according to other literatures [31,32],  $b$  was taken as 1 m in the entire simulations) and prescribed to be permeable, representing the arrangement of PVDs. For a given depth

of overlapping water  $h$  on the soil, the linearly increasing hydraulic pressure was specified by the field variables of PORE in ABAQUS through the soil domain. Meanwhile, to represent the contribution of overlapping water to improving soil, an additional suction head  $-h_{\text{add}}$  was introduced and superposed in the reference suction head  $-h_{\text{v,ref}}$ . In this study,  $-h_{\text{v,ref}}$  was taken as  $-8.5$  m associated with a reference negative pressure of  $-85$  kPa, referred to an vacuum loss in practice [33,34].  $h_{\text{add}}$  should not be larger than  $h$ , and the equivalent suction head  $-h_{\text{v}} = -(h_{\text{v,ref}} + h_{\text{add}})$  corresponds to the required water head of submerged pump. For instance, when the lowest water depth  $h$  (note, the proper capacity of submerged pump is assumed to be adopted according to the lowest astronomical tide level, hence the change in water depth does not influence the magnitude of suction) is equal to  $10$  m, associated with the condition of lowest water sea level, the maximum equivalent suction head assigned to the PVDs' nodes can be taken as  $-18.5$  m corresponding to a negative pressure of  $-185$  kPa.

An example of a finite element model with  $B/H = 1$  in this study is shown in Figure 1 with total elements of 16,940. The soil was represented as deformable body with first-order full integration stress–pore fluid continuum elements (ref. type CPE4P, in the standard ABAQUS library). Noted that, two-dimensional (2D) FE analyses were carried out with the configuration of multi-drains, considering a similar response of settlement from plain strain and three-dimensional (3D) analyses [35,36]. The sensitivity study of mesh density was implemented to ensure a computationally efficient mesh and satisfactory accuracy. The whole soil domain had a breadth of  $11B$  and a depth of  $5H$  beneath the improved soil region to ensure a negligible boundary effect. The base of mesh was fixed while the lateral boundary was given to the horizontal displacement. The configuration (drainage and freedom boundary) of surface at the top of soil domain aside the improved soil region differs from analysis scenarios, and more details is described in the Section 2.3.

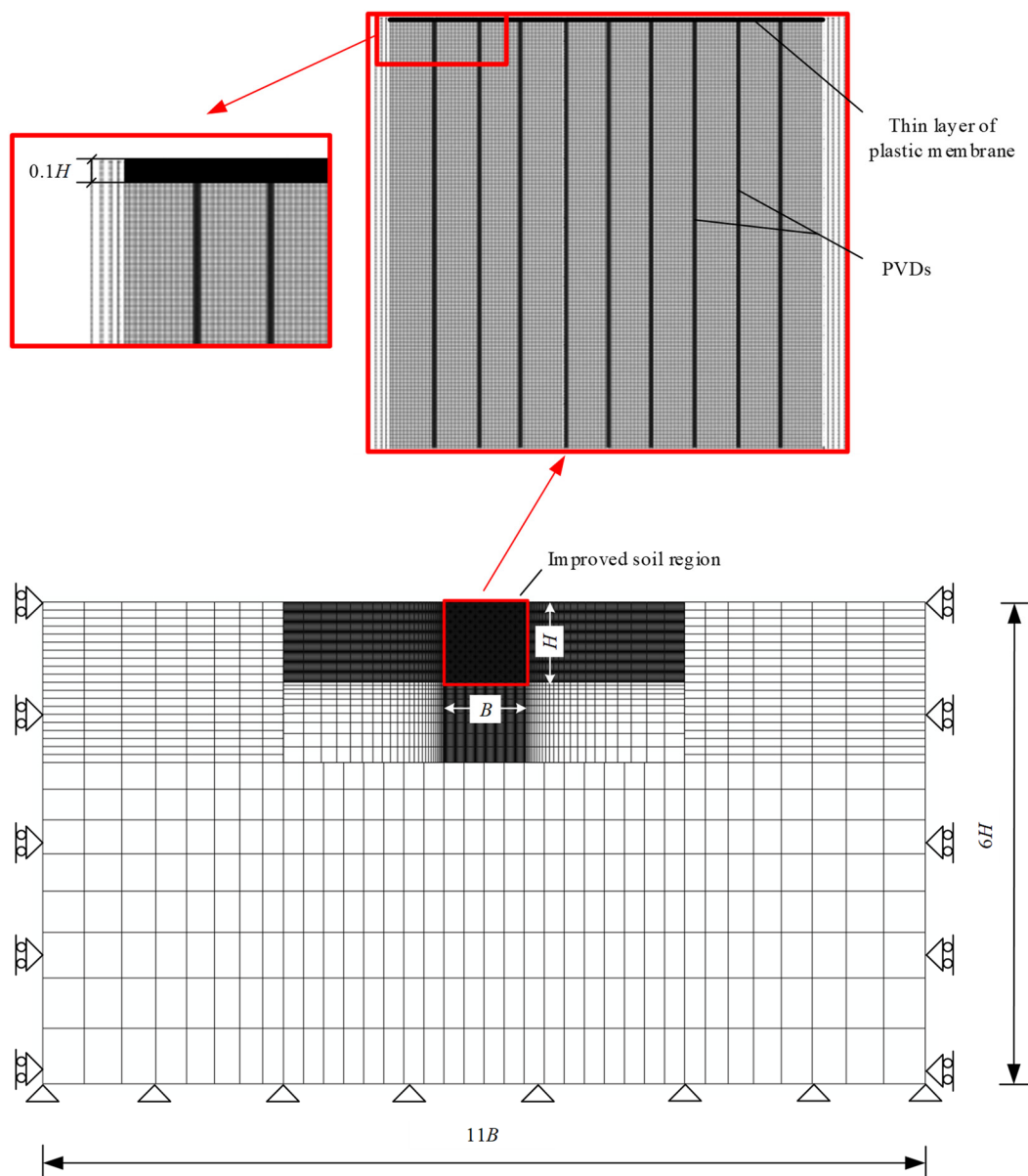


**Figure 1.** FE model with boundary condition and mesh technology.

### 2.2. Soil Parameters

The soil was prescribed as a homogenous, isotropic, and linearly elastic half space with Biot consolidation theory allowing the stress-pore fluid coupling. Therefore, only two elastic parameters, Young’s modulus  $E$  and Poisson’s ratio  $\nu$ , were defined through the analyses. However, the anisotropy of permeability was considered with the ratios of horizontal to vertical permeability  $k_h/k_v = 1, 2, \text{ and } 3$  in accordance with other literatures [28,37–39].

Although the magnitude of  $\nu$  can affect the consolidation behavior, e.g., the higher the Poisson’s ratio, the faster the consolidation and lower consolidation settlement [40,41], such effect is limited [41,42] in a practical range of drained Poisson’s ratio  $0.1 \leq \nu \leq 0.3$ . Here, according to the study from other literatures [2,39,43],  $\nu$  was taken as 0.3 and a typical value of one-dimension compressive modulus  $E_s = 2.74 \text{ MPa}$  [5,43] was adopted in this study. These represent the nature of the typical marine clay, especially at the shallow depth in the seafloor [39,43].

The elastic Young's modulus  $E$  can be captured by

$$E = E_s \frac{(1 - 2\nu)(1 + \nu)}{1 - \nu}, \quad (1)$$

The value of vertical permeability  $k_v = 1.16 \times 10^{-10}$  m/s was chosen [43], so the operative consolidation coefficient  $c_{vh}$  is

$$c_{vh} = \frac{kE}{\gamma_w} \frac{1 - \nu}{(1 - 2\nu)(1 + \nu)}, \quad (2)$$

where,  $k$  is the effective permeability of soil, defined by

$$k = \sqrt{k_v k_h} \quad (3)$$

All parameters relevant to the drained analysis in this study are illustrated in Table 1, and all the values were taken according to other literatures [2,5,28,37–39,43,44].

**Table 1.** Soil parameters for numerical study.

Soil Property Parameters	Values
Submerged unit weight of soil, $\gamma'$ (kN/m <sup>3</sup> )	6
Unit weight of water, $\gamma_w$ (kN/m <sup>3</sup> )	10
One-dimension compressive modulus, $E_s$ (MPa)	2.74
Young's modulus, $E$ (MPa)	2.04
Poisson's ratio, (-)	0.3
Vertical permeability, $k_v$ (m/s)	$1.16 \times 10^{-10}$
Vertical consolidation coefficient, $c_v$ (m <sup>2</sup> /s)	$3.17 \times 10^{-8}$

### 2.3. Scope and Loading Conditions

Three types of simulation schemes were implemented to examine the effects of consolidation and seepage on the soil settlement due to the existence of overlapping water in the process of underwater vacuum preloading. The top surface of soil domain was set as the impermeable boundary. Then a given suction (i.e., a suction head  $-h_v$  corresponds to a negative pressure of  $\Delta u = -\gamma_w h_v$ ) was applied to each node along the vertical edges representing the drainage-allowable PVDs within the improved soil region. Following the foregoing set-up of numerical model, the consolidation was then allowed until no excess pore pressure existed in the entire soil domain. This is the first type of simulation scheme, namely suction-induced consolidation analysis (scheme I, see Figure 2a). Noted here, it is an idealized scenario, since the impermeable top surface aside the improved soil region was artificially implemented, aiming to avoid any seepage flow from the overlapping water into the improved soil zone involved in the analysis. Another one is suction-induced seepage analysis (scheme II) where the top surface of soil domain was restrained without any movement, and the drainage was permitted cross the surfaces besides the improved soil region (see Figure 2b). The third one is the analysis with the combination of suction-induced consolidation and seepage (scheme III, see Figure 2c). The only difference of the last two types of analyses is the elimination of constraint of the top surface as the free boundary again.

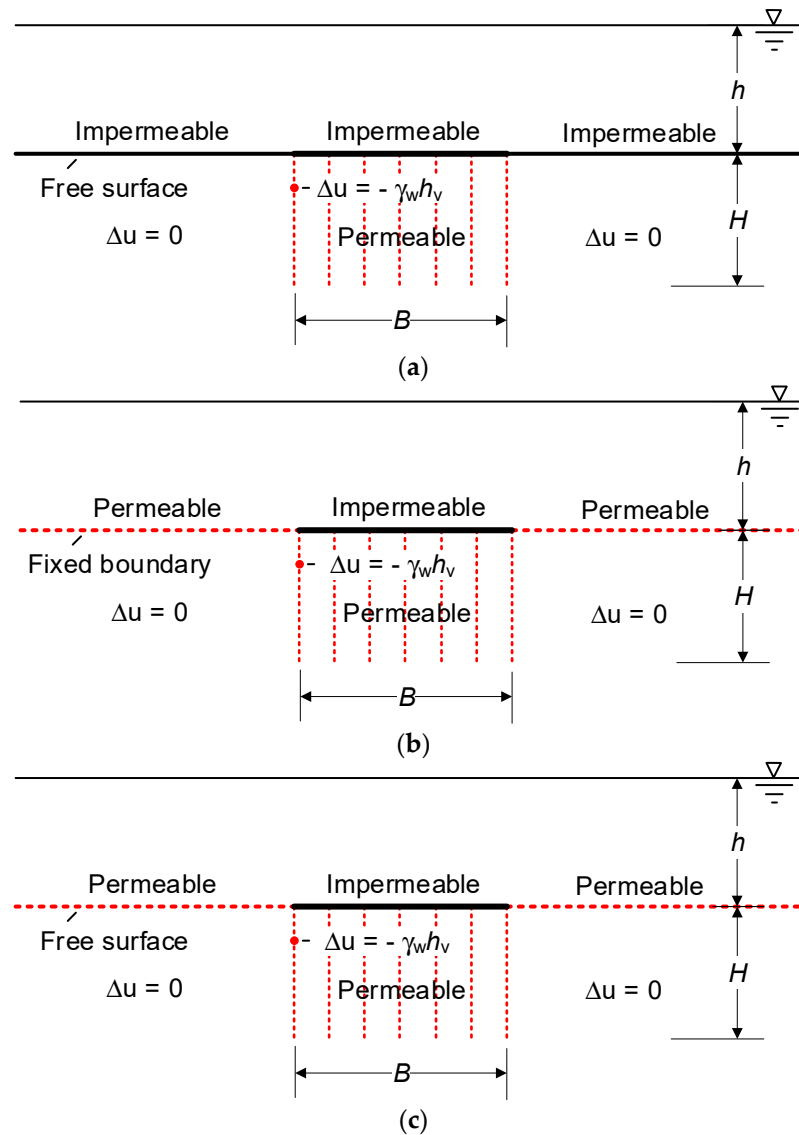


**Figure 2.** Drainage boundary and loading conditions in three analysis schemes: (a) Scheme I Suction-induced consolidation analysis; (b) Scheme II Suction-induced seepage analysis; (c) Scheme III Combination analysis.

In these types of analyses scenarios, the parametric study was conducted, with a group of normalized quantities considered. They are the aspect ratio of improved soil region  $B/H$ , the ratio of suction head  $-h_v/H$ , and anisotropic ratio of permeability  $k_h/k_v$ . The entire simulation scheme is illustrated in Table 2. Note, all parametric studies are based on the non-dimensional groups of parameters, with increasing  $B/H$  representing the square, rectangular, and strip shapes of improved soil regions respectively, with increasing  $h_v/H$  representing the deeper water depth, with increasing  $k_h/k_v$  representing the faster horizontal drainage rate ( $k_h/k_v$  is generally within 1 to 10 for the typical marine clay [43] and 1 to 3 is usually seen in practice [2,39,43]).

**Table 2.** The numerical simulation schemes

Analysis Schemes	Influence Factors		
	$B/H$	$-h_v/H$	$k_h/k_v$
Suction-induced consolidation (Scheme I)			
Suction-induced seepage (Scheme II)	1, 5, 10, 20	-0.85, -0.95, -1.35, -1.85, -2.35	1, 2, 3
Combination of suction-induced consolidation and seepage (Scheme III)			

The adoption of the initial time step is of interest in drained analysis to ensure a stable build-up of initial pore pressure without the missing or distortion of subsequent consolidation response. The minimum value of initial time step  $t_{init}$  was prescribed by [45].

$$t_{init} = \Delta l^2 \frac{\gamma_w}{6Ek'}, \tag{4}$$

where,  $\Delta l$  is the characteristic element length taken as 0.01 m around the PVDs in this paper.

*2.4. Model Validation*

Following the study of [43] on the consolidation behavior of strip foundation subjected to a vertical surcharge load, the dissipation responses of excess pore pressure at the topsoil along the centreline were compared. Here, the finite element mesh strategy of this study was used, but the thin layer with the width of  $B$  on the top of improved soil was specified as rigid body without the application of suction head along the PVDs' edges. As evident from Figure 3, a good agreement can be observed from normalized change in excess pore pressure  $\Delta u / \Delta u_i$  against elapsed time factor  $T = c_{vh}t / B^2$ .  $\Delta u$  is the dissipated excess pore pressure with time, and  $\Delta u_i$  is the initial excess pore pressure. Therefore, the mesh technology and configuration of the numerical model reported in this paper can be validated to be used in the further drained analysis.

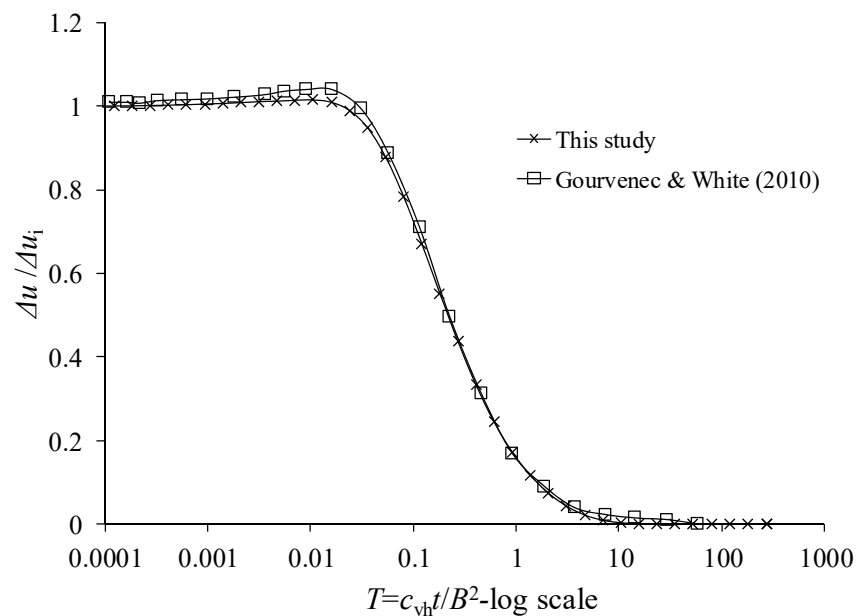


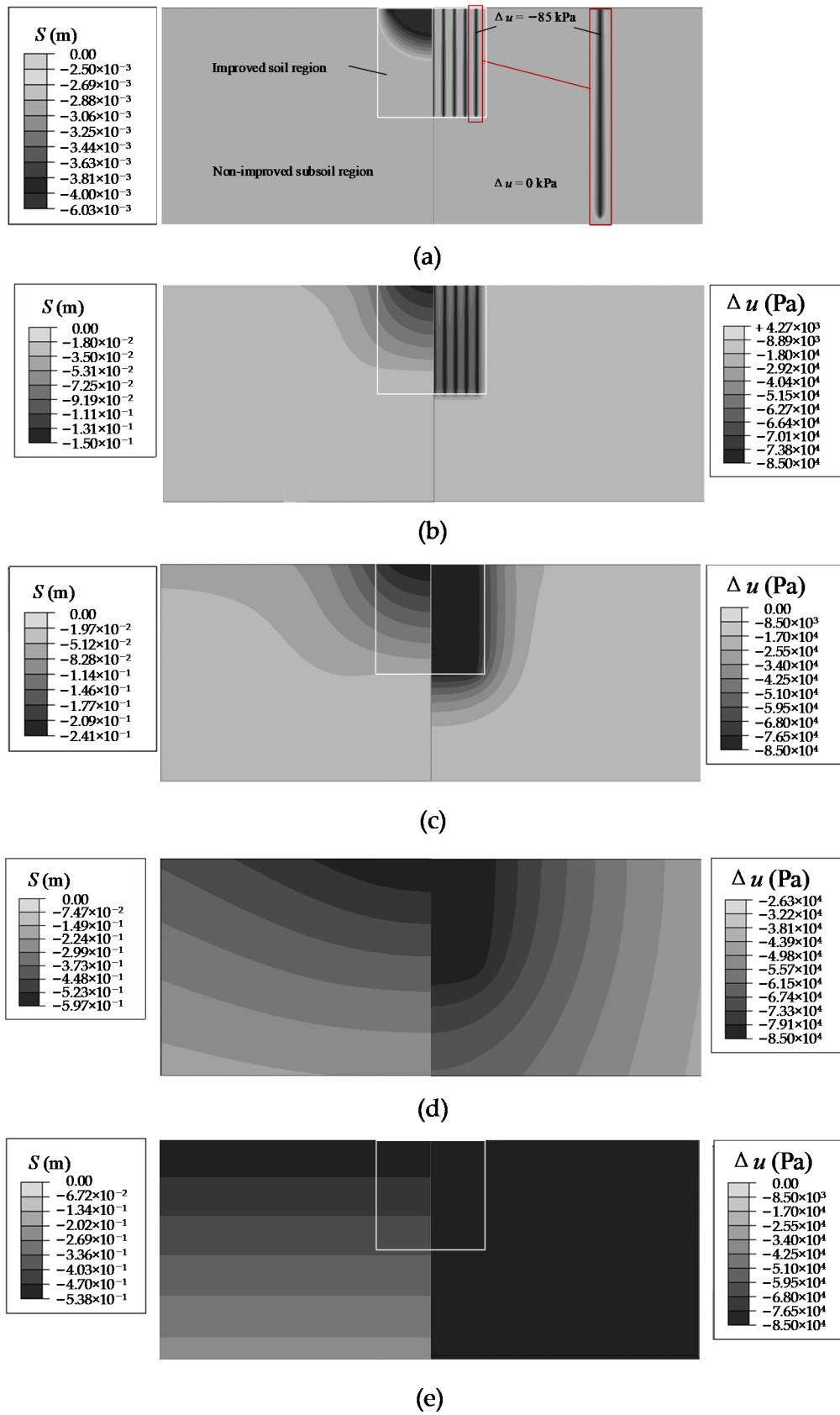
**Figure 3.** Model validation by comparing excess pore pressure dissipation curves.

### 3. Numerical Analysis Results

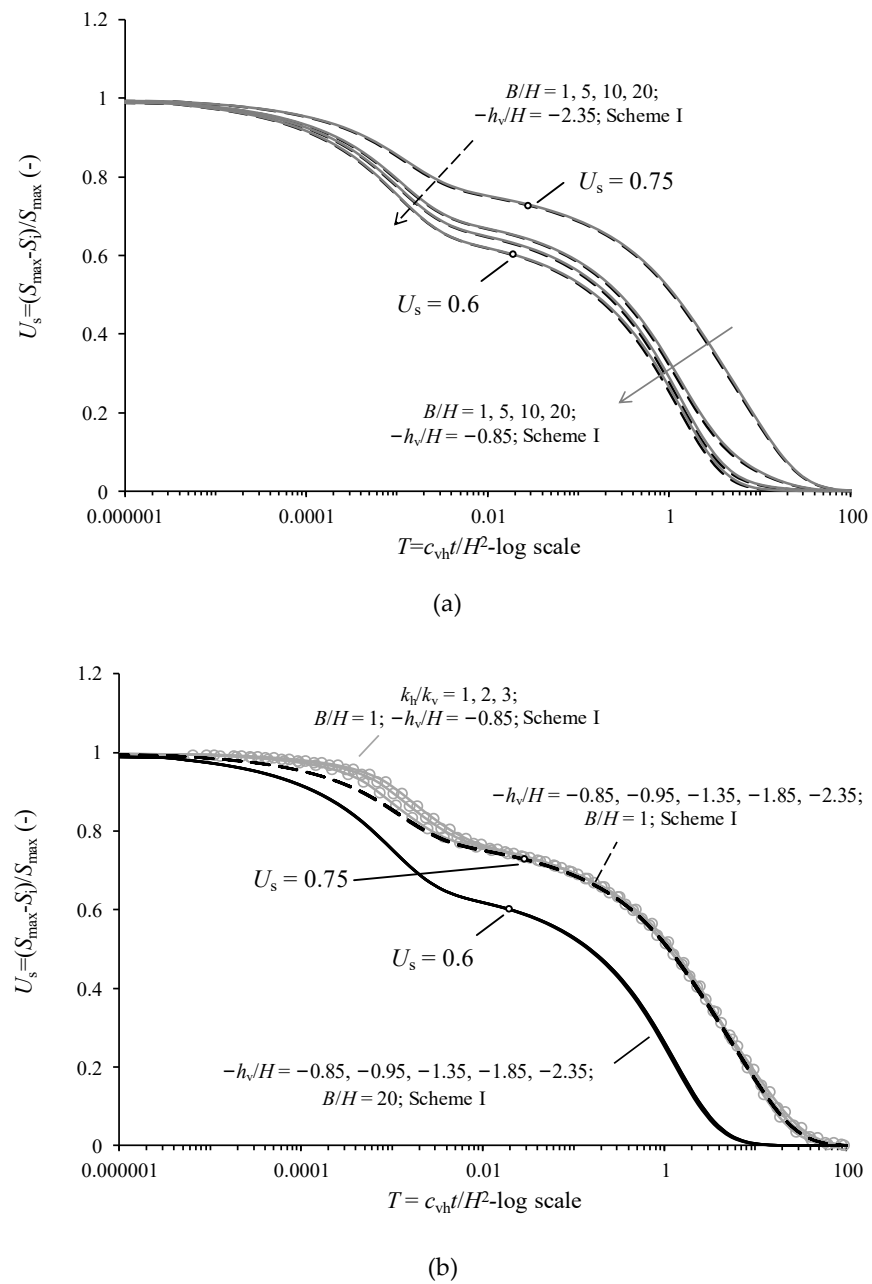
#### 3.1. Simulated Settlement in the Suction-Induced Consolidation Scheme

Figure 4 shows the evolution of settlement in response to the dissipation of excess pore pressure  $\Delta u$  during the process of suction-induced consolidation. Only the case of  $B/H = 1$ ,  $-h_v/H = -0.85$ , and  $k_h/k_v = 1$  was demonstrated here, due to the similarity of evolution mechanism among the simulated cases. Five typical phases during the consolidation can be summarized: (i) onset of applying the specified suction head along the PVDs ( $T = 0$ , see Figure 4a). A series of discrete negative pressure regions shaped in ribbon pattern were generated, and the soil around PVDs slightly settled (Figure 4a). (ii) Transient phase with consolidation mainly occurring in the improved soil region ( $T = 0.002$ ; see Figure 4b). The negative excess pore pressure was starting to expand mainly within the improved soil region, yet the settlement outside the improved soil zone occurred. (iii) Completion of consolidation in the improved soil region ( $T = 0.061$ ; see Figure 4c). After the duration of consolidation of  $t = 1.94 \times 10^8$  s (corresponding to  $T = 0.061$ , around 6.15 years), the entire improved soil region showed a uniform negative  $\Delta u$  of  $-85$  kPa, indicating the completion of consolidation within the improved soil region. It is consistent with the response of displacement (the legend  $S$  for the settlement) contour, where the soil settlement mainly occurred in the improved soil zone. The soil aside the improved region also performed the observable settlement, while the soil below the improved region performed the neglectable settlement. It is attributed to the difference in drainage path, shorter for the sideward soil, longer for the subsoil. (vi) Transient phase with ongoing consolidation mainly occurring in the non-improved soil region ( $T = 5.273$ ; see Figure 4d). The negative pore pressure was gradually expanding to far field, with the settlement aside and beneath the improved soil regions generated. (v) Completion of consolidation in the entire soil domain ( $T = 2738$ ; see Figure 4e). With the continuous maintaining of suction head,  $\Delta u$  of  $-85$  kPa propagated in the entire soil domain ( $t = 8.64 \times 10^{12}$  s associated with  $T = 2738$ ), reflecting the accomplishment of suction-induced consolidation. It resulted in a uniform settlement through the soil domain.

To investigate the influences of  $B/H$ ,  $-h_v/H$ , and  $k_h/k_v$  on the settlement due to suction-induced consolidation, response of the normalized consolidation settlement ( $U_s = (S_{\max} - S_i)/S_{\max}$ ) at the top surface and along the centreline of soil domain against the normalized elapsed time ( $T = c_{vh}t/H^2$ ) is reported in Figure 5a,b, where  $(1 - U_s)$  is the consolidation degree in the formation of settlement,  $S_i$  is the current consolidation settlement, and  $S_{\max}$  is the final settlement after full consolidation. Four different  $B/H$  (of 1, 5, 10, and 20), five different  $-h_v/H$  (of  $-0.85$ ,  $-0.95$ ,  $-1.35$ ,  $-1.85$ , and  $-2.35$ ), and three different  $k_h/k_v$  (of 1, 2 and 3) were included. The significant transition phase can be observed at  $U_s$  of around 0.6 to 0.75 in all simulated cases. It is consistent with the evolution mechanism of settlement described above, where the settlement mainly occurred in the improved soil region at the early stage then in the subsoil, due to the difference in the length of drainage path. For identical  $B/H$ , the consolidation curves were almost coincident with varying  $-h_v/H$  and  $k_h/k_v$ , implying no impact on them. As  $B/H$  increased, a faster rate of consolidation was found, with less discrepancy in larger  $B/H$ . It is reasonable since more PVDs can be employed in the case of larger  $B/H$ , resulting in the larger drain section and higher efficiency in drainage. It may imply that an efficient dimension for the improved soil region could be satisfied as  $B/H \geq 5$ .



**Figure 4.** The evolution of settlement in response to the dissipation of excess pore pressure  $\Delta u$  during the process of suction-induced consolidation: (a)  $T = 0$ ; (b)  $T = 0.002$ ; (c)  $T = 0.061$ ; (d)  $T = 5.273$ ; (e)  $T = 2738.88$ .



**Figure 5.** The response of the normalized consolidation settlement ( $U_s = (S_{max} - S_i) / S_{max}$ ) at the central point along the top surface of improved soil region against the normalized elapsed time ( $T = c_{vh}t / H^2$ ): (a) varied  $B/H$ ; (b) varied  $-h_v/H$ .

3.2. Simulated Flow in the Suction-Induced Seepage Scheme

Figure 6a shows the development of suction-induced seepage with respect to the dissipation of excess pore pressure  $\Delta u$  for the case of  $B/H = 1$ ,  $-h_v/H = -0.85$  and  $k_h/k_v = 1$ . The region extending a distance of to  $2H$  horizontally and  $H$  vertically from the boundary of improved soil zone was selected, as the quantity of seepage flow into the improved region was of greatest practical interest. From the distribution of  $\Delta u$  at the very onset ( $t = 2.95 \times 10^{-5}$  s corresponding to  $T = 9.36 \times 10^{-5}$ ), as seen in Figure 6(a-1), a  $\Delta u$  of  $-85$  kPa was generated as expected along the PVDs, resulting in the pore flow confined in the vicinity of PVDs along the horizontal direction. The seepage zones gradually extended to the unimproved soil part, as the suction head held. At  $t = 5.75 \times 10^7$  s (associated with  $T = 0.018$ ), as shown in Figure 6(a-2), the different magnitude of head loss was observed through the soil domain, with the largest head loss ( $\Delta u = -85$  kPa)

occurring in the improved soil region, with the constant-head boundary ( $\Delta u = 0$ ) slightly extending downward. It led to the obvious seepage flow from constant-head boundary to the improved soil zone. After a period of  $t = 1.12 \times 10^{10}$  s (associated with  $T = 3.55$ ), the steady-state seepage approached with the unchanged contour of  $\Delta u$  and distribution of flow velocity vector (see Figure 6(a-3)). Regarding the  $H \times H$  zone aside the improved soil region, the seepage seemed to occur along a locus of quadrant. Regarding the bottom boundary of the improved soil region, the seepage inflow seemed to experience a longer path from the constant-head boundary.

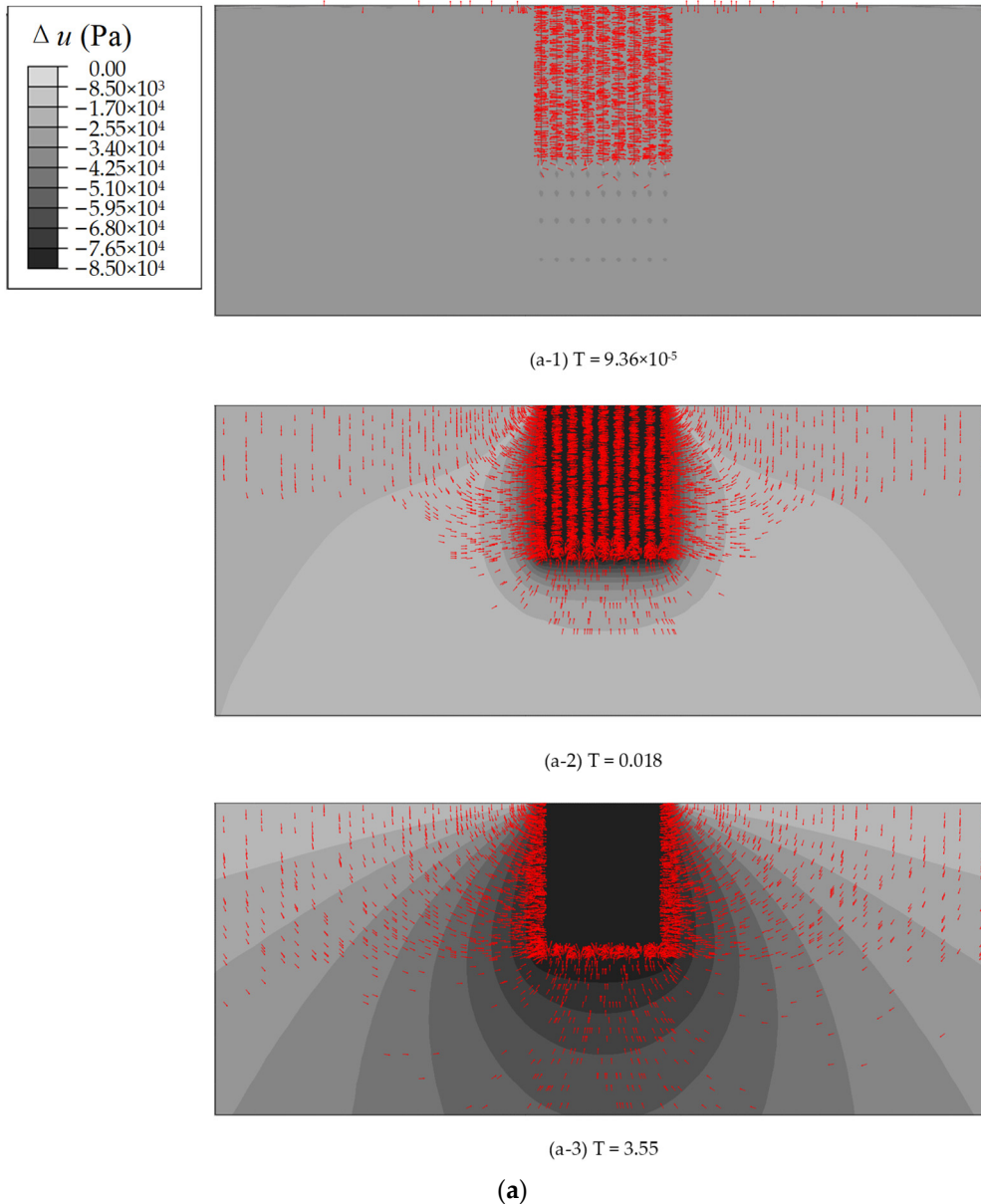
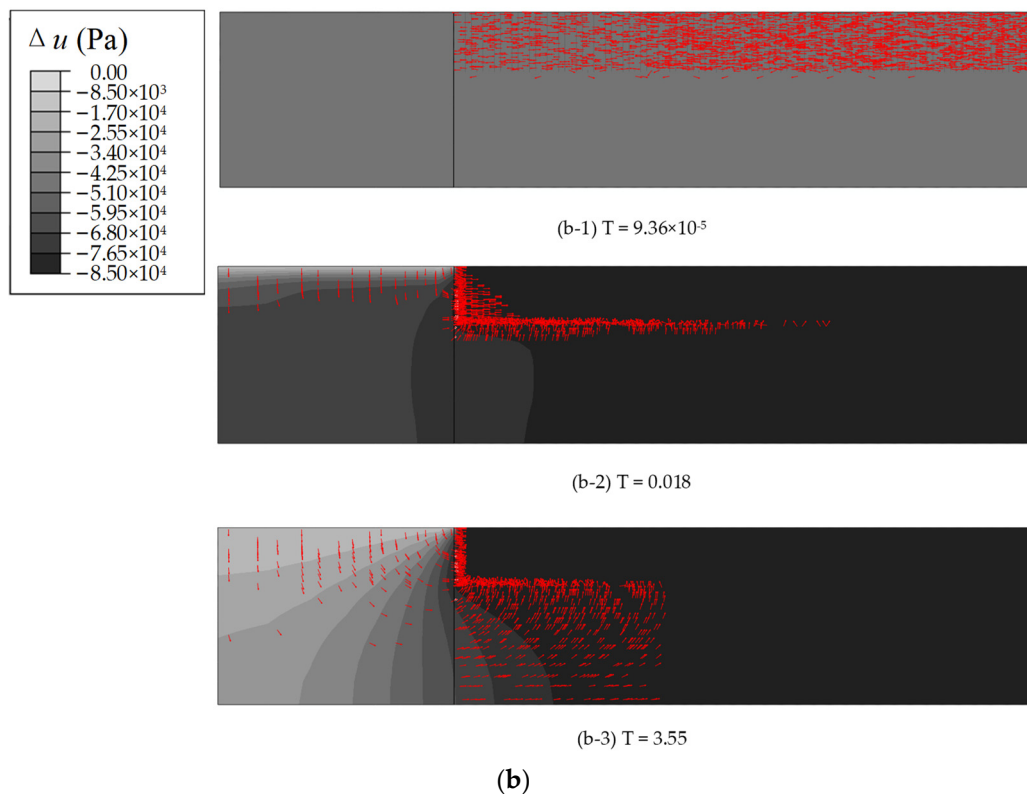


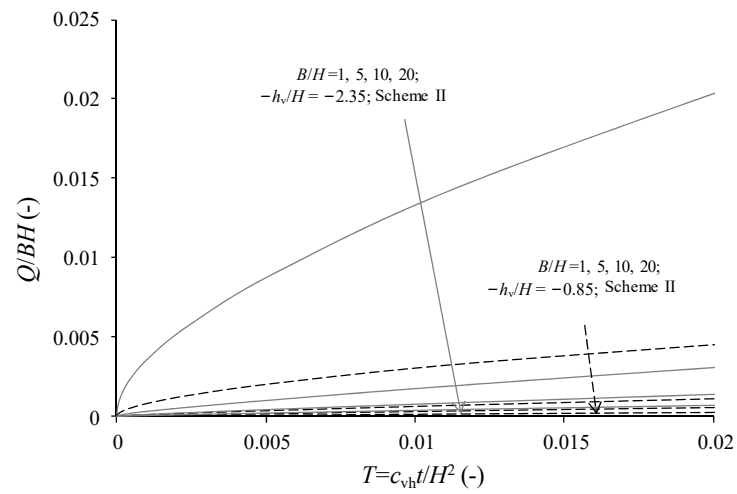
Figure 6. Cont.



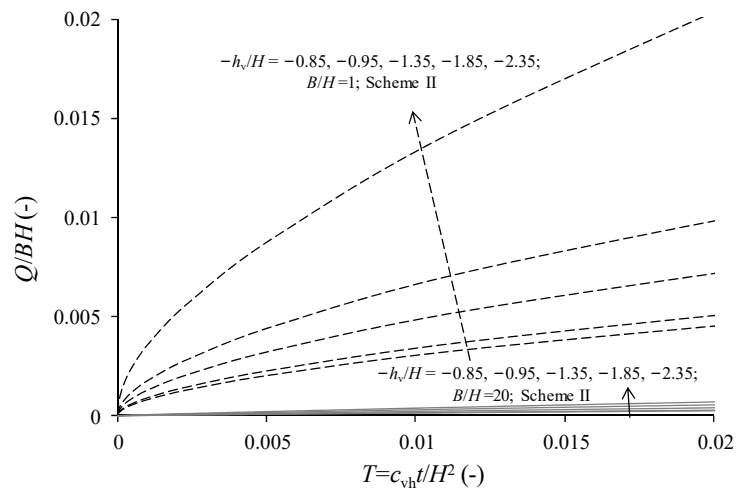
**Figure 6.** The development of suction-induced seepage with the dissipation of excess pore pressure  $\Delta u$ : (a)  $B/H = 1$ ; (b)  $B/H = 20$ .

Comparison of Figure 6a,b shows that, despite the difference in geometry of the improved soil region (a wider improved soil zone with same height in Figure 6b), the seepage flow appeared to develop following a similar pattern. It comprised of three stages: build-up of the low-constant-head (suction), evolution of head loss (transitional stage), and steady-state seepage flow. The significant difference in them is along the bottom boundary of improved soil region, where the remarkable flow occurred only in the two corner zones.

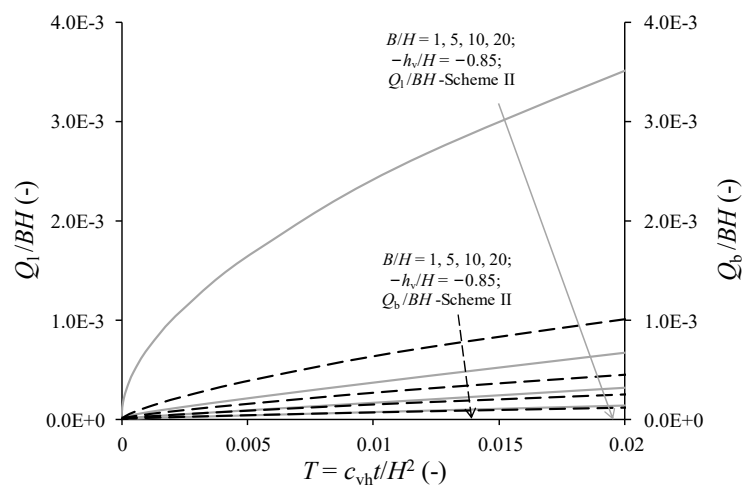
To examine the seepage flow of both lateral and bottom boundary of improved soil region, the seepage discharge  $Q$  normalized by  $BH$  against the elapsed time factor  $T = c_{vh}t/H^2$  is reported in Figure 7. The term  $Q/BH$  in fact reflects the operative seepage discharge into the improved soil region due to suction, and  $Q_l/BH$  and  $Q_b/BH$  are for lateral and bottom seepage flow, respectively. All discharge curves appeared to have a similar trend, with a short sharp rise following a quite linear increase. It was consistent with the two typical stages described above, one for transitional stage, another for steady-state stage. Regarding the variation of discharges ( $Q/BH$ ,  $Q_l/BH$ , and  $Q_b/BH$ ) with different parameters, it can be seen that, the quantity of water flowing into the improved soil region increased as the suction head  $-h_v/H$  was elevated, and decreased with the increasing of  $B/H$ .  $Q_b/BH$  was lower than  $Q_l/BH$  in general when  $B/H$  and  $-h_v/H$  were identical. It is important to realize that, as  $B/H$  increased, the operative discharge did not show a rise and instead a degradation, although more PVDs were implemented with a wide range of suction applied. This can be well explained by the previous observation that the seepage at the bottom boundary of improved soil region was found only in the limited corner zone.



(a)



(b)



(c)

Figure 7. The normalized operative seepage discharge  $Q/BH$  with the elapsed time factor  $T = c_{vh}t/H^2$ : (a)  $B/H$ ; (b)  $-h_v/H$ ; (c)  $Q_1/BH$  and  $Q_b/BH$ .

### 3.3. Simulated Settlement in the Combination of Consolidation and Seepage Scheme

This section considers the realistic scenario involved in the underwater vacuum preloading, where both the consolidation and seepage occur simultaneously and impact the settlement throughout the improved soil region. Insights into the mechanism are reported in Figure 8, where the settlement in the soil region of concern accompanied by the distribution of excess pore pressure  $\Delta u$  is considered. The selected simulation time (here,  $t = 8.64 \times 10^{12}$  s associated with  $T = 2738$ ) is sufficiently long to ensure the seepage is under steady state. From comparison with the mechanisms under only suction-induced consolidation or seepage (described in the last two sections), the main findings followed: (1) Compared to the uniform settlement in scheme I, the considerable nonuniform settlement along the top surface of improved region can be found, in particular, in the region close to both sides; (2) compared to the flow paths (flow velocity vector field) in scheme II, the similar seepage zone can be observed in the cases with high  $B/H$ , which was restricted in the whole lateral boundary and part of bottom boundary (around  $B/3$ ) of improved soil region. These may be explained by the existence of seepage flow. It showed that the suction head applied within the improved soil region, in particular close to both sides, not only acted as the consolidation pressure, but also pumped the seepage inflow out of the PVDs. The seepage flow therefore led to a decrease in effective consolidation pressure in a certain improved soil region, or perhaps can be thought as a “negative” settlement in the limited region, and thus a nonuniform settlement along the soil surface.

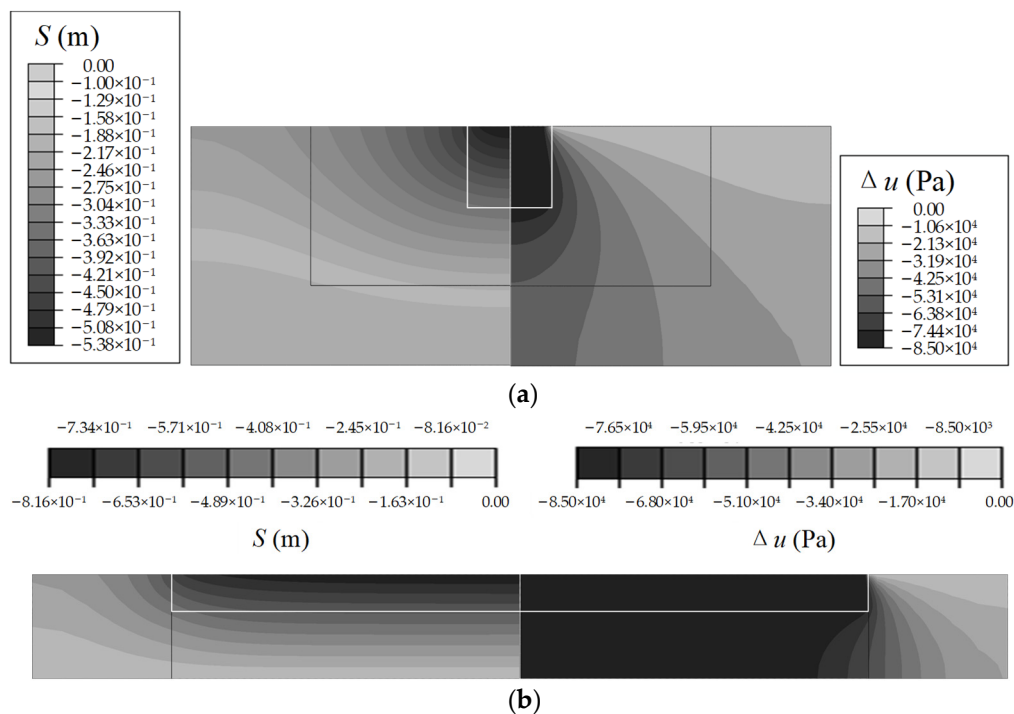


**Figure 8.** The response of settlement in the soil region of concern accompanied by the distribution of excess pore pressure  $\Delta u$  at  $T = 2738$ : (a)  $B/H = 1$ ; (b)  $B/H = 20$ .

Figure 9 presents a suite of responses of history settlement for the position located at the top surface of soil along the centreline. Results from the analyses in schemes I and III are included, with varying  $B/H$  and  $-h_v/H$ . It is clear that, two piecewise responses were obvious, because of different consolidation rate in the region of improved soil and bottom soil. All curves merged into an identical trend, which fell adjacent to the response of the case with  $B/H = 20$ . It was consistent with the observation described above. Under larger  $B/H$ , the influence of seepage flow can be neglected for the central region of improved soil zone, so the settlement responses from schemes I and III were almost same. But under

lower  $B/H$ , the seepage flow resulted in a reduction of effective consolidation pressure, and thus a lower value in the final settlement  $S_{max}$  even at the central region, which led to a faster consolidation response and close to a non-seepage response.

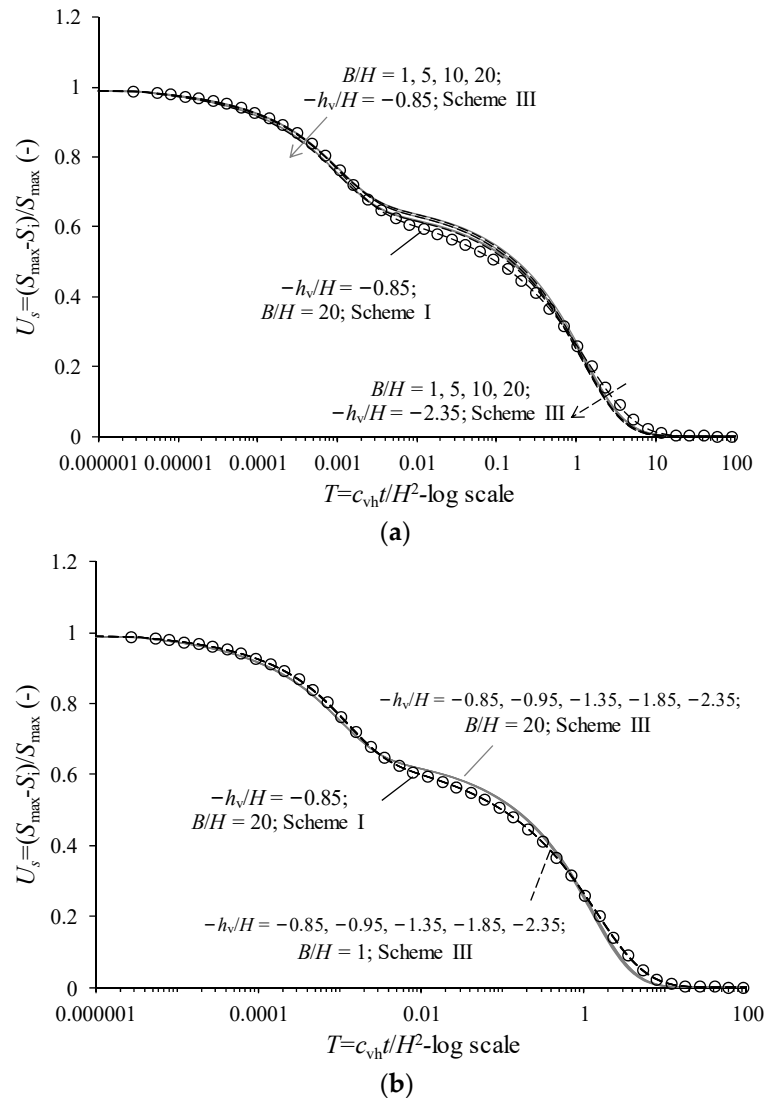


**Figure 9.** The responses of history settlement for the position located at the central point along the top surface of improved soil region: (a)  $B/H$ ; (b)  $-h_v/H$ .

Such influence from the seepage flow on the settlement is illustrated in Figure 10 with two different consolidation degrees ( $1 - U_s$ ) of 40% and 99% included. They are representations of the routine time of applying vacuum in practice (around 3–6 months) and the time when suction-induced settlement (including both improved soil and subsoil regions) almost completed. As evident from Figure 10, a significant nonuniform settlement appeared at the top surface of improved soil, with the maximum at the center ( $x/B = 0$ ) and the minimum on both sides ( $x/B = \pm 0.5$ ). The magnitude of nonuniform settlement increased with increasing  $B/H$  and  $(1 - U_s)$ . This implied that the “negative” settlement induced by seepage flow compensated a part of consolidation settlement because of reduction in effective consolidation pressure, and its influence zone differed from  $B/H$  with more “negative” settlements close to lateral boundary of improved soil region. It can be demonstrated from a further comparison with settlement obtained in scheme I (see Figure 10b). The final settlement at the center in scheme III was almost equal to that in

scheme I at  $B/H = 20$ , indicating the influence of seepage on the central settlement along the top surface of improved soil could be neglected under sufficiently large  $B/H$ .

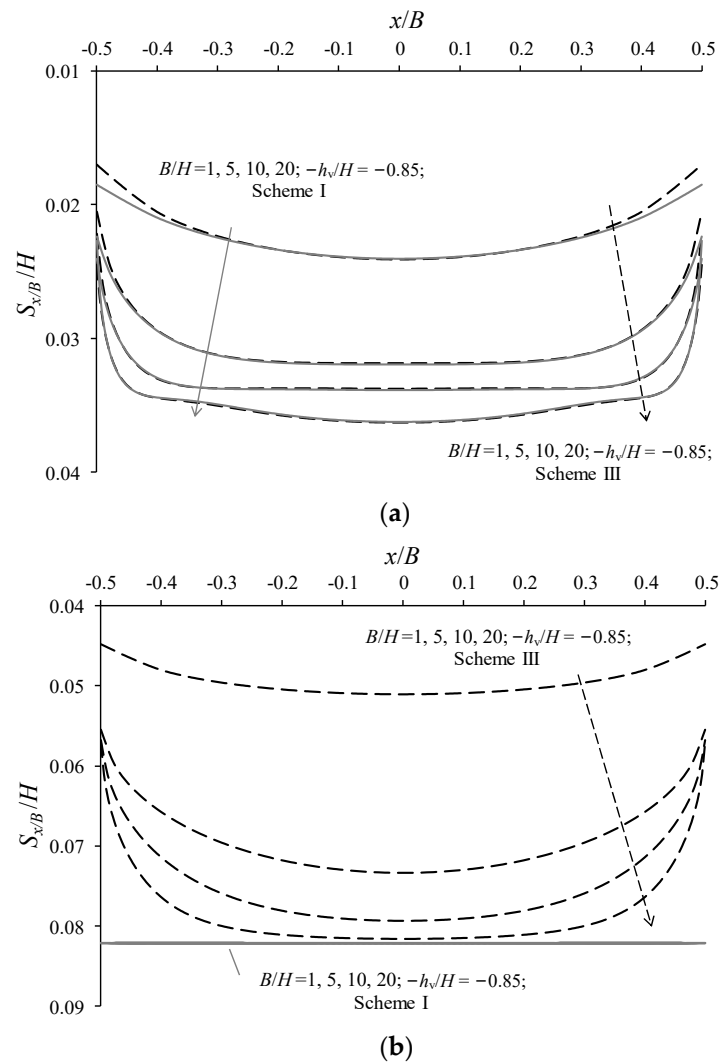


**Figure 10.** Comparison of non-uniform settlements at the consolidation degrees  $(1 - U_s)$  of 40% and 99%: (a)  $1 - U_s = 0.4$ ; (b)  $1 - U_s = 0.99$ .

#### 4. Back-Calculated Approach to Predict the Settlement

##### 4.1. Prediction of Consolidation Settlement without Consideration of Seepage

Considering the minimum influence of seepage on the settlement of central point at the top surface of improved soil under large  $B/H$  (i.e.,  $B/H = 20$ ), its estimation was implemented here, with contributions from both improved soil and non-improved subsoil regions included.

The settlement at the central point of topsoil surface  $S_i$  can be expressed as

$$S_i = S_{i1} + S_{i2}, \tag{5}$$

where  $S_{i1}$  and  $S_{i2}$  are the corresponding settlements for the improved soil and non-improved subsoil regions, respectively.

For the improved soil region,  $S_{i1}$  can be computed following the expression proposed by [46]

$$S_{i1} = S_{i1,max}(1 - U_{s1}) = \frac{\gamma_w h_v H}{E_{s1}} [1 - (1 - U_{h1})(1 - U_{v1})], \tag{6}$$

where  $S_{i1,max}$  is the final settlement of the improved soil region, and  $(1 - U_{s1})$  and  $\bar{E}_{s1}$  are the corresponding equivalent consolidation degree and constrained modulus through the improved soil strata.

$U_{h1}$  in Equation (6) is the consolidation degree due to the horizontal drainage, and can be calculated by the expression provided by [12,22].

$$U_{h1} = 1 - \exp\left[-\frac{8}{F(n)}T_h\right], \tag{7}$$

where

$$T_h = \frac{c_h t}{(0.4D_e)^2}, \tag{8}$$

$$F(n) = \frac{n^2}{n^2 - 1} \ln n - \frac{3n^2 - 1}{4n^2}, \tag{9}$$

where,  $0.4D_e$  is the equivalent drainage path under 2D condition, and  $F(n)$  is the equivalent horizontal drainage path,  $n = D_e/D_w$ , with  $D_w$  for the diameter of the drains.

$U_{v1}$  in Equation (6) is the consolidation degree due to the vertical drainage only for the improved soil region, and can be expressed with a simplified formation following the one-dimensional consolidation theory [47].

$$U_{v1} = 1 - \frac{8}{\pi^2} \exp\left(-\frac{\pi^2}{4}T_{v1}\right), \tag{10}$$

where

$$T_{v1} = \frac{c_v t}{H^2}, \tag{11}$$

For non-improved subsoil region,  $S_{i2}$  was calculated referring to Terzaghi's theory of 1D consolidation [47]

$$S_{i2} = S_{i2,max}(1 - U_{s2}) = \frac{\gamma_w h_v H_b}{\bar{E}_{s2}}(1 - U_{v2}), \tag{12}$$

and

$$U_{v2} = 1 - \frac{8}{\pi^2} \exp\left(-\frac{\pi^2}{4}T_{v2}\right), \tag{13}$$

$$T_{v2} = \frac{c_v t}{(m_d H_b)^2}, \tag{14}$$

where,  $S_{i2,max}$  is the final settlement of the non-improved subsoil region;  $(1 - U_{s2})$  and  $\bar{E}_{s2}$  are the corresponding equivalent consolidation degree and constrained modulus;  $H_b$  is the depth of subsoil;  $U_{v2}$  is the consolidation degree due to vertical drainage. Noted that the term of  $m_d H_b$  is the modified drainage path (here  $m_d$  around 0.5), which represents a discontinuous drainage boundary (discrete PVDs) rather than a continuous drainage boundary in the Terzaghi's theory.

Combining Equation (5), Equation (6), and Equation (12), yields the normalized settlement of central point at the top surface of soil domain  $U_s$ .

$$U_s = 1 - \frac{S_i}{S_{i1,max} + S_{i2,max}} = \frac{\bar{E}_{s2}H(1 - U_{h1})(1 - U_{v1}) + \bar{E}_{s1}H_b U_{v2}}{\bar{E}_{s2}H + \bar{E}_{s1}H_b}, \tag{15}$$

The results computed by Equation (15) were compared with the consolidation curve of  $B/H = 20$  obtained from FE analysis in scheme I or III (because of their similarity described earlier). As shown in Figure 11, a quite good agreement can be observed, implying the modification on the drainage path functioned well to represent two piecewise consolidation rates. Note, there is an observable difference of results from Equation (15) and FE analysis at T from 0.002 to 5.317. It may be attributed to the fact that a simplified method based on

the one-dimensional consolidation theory is used to estimate the consolidation settlement of non-improved soil region.

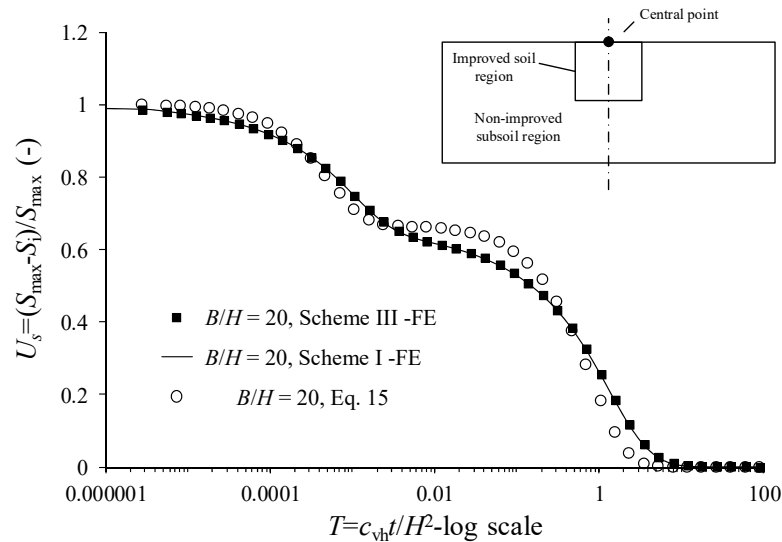


Figure 11. Comparison of normalized settlement responses between the numerical and calculated results.

#### 4.2. Prediction of the Operative Seepage Discharge

With the retrospection of suction-induced seepage mechanism discussed previously, the simplified flow paths were established as shown in Figure 12. For a given depth  $z$  (see Point  $A_1$ ) along the lateral boundary of improved soil region, the flow path was assumed to be a quarter of circle with a length of  $\pi z/2$ , and for a given position  $z'$  ( $\leq H/2$ ) away from the corner along the bottom boundary (see point  $B_1$ ), the flow path was assumed to be a combination of a quarter of circle with a length of  $\pi(z + z')/2$  and another quarter of circle with a length of  $\pi z'/2$ . Here, the region of occurring seepage was artificially confined within the width of  $3H/2$  aside the improved soil zone. However, the flow paths can be used to calculate a reference discharge along both lateral and bottom boundaries, with two satisfactory assumptions (1) the soil is fully saturated; (2) the seepage is stable state flow conforming to Darcy’s law.

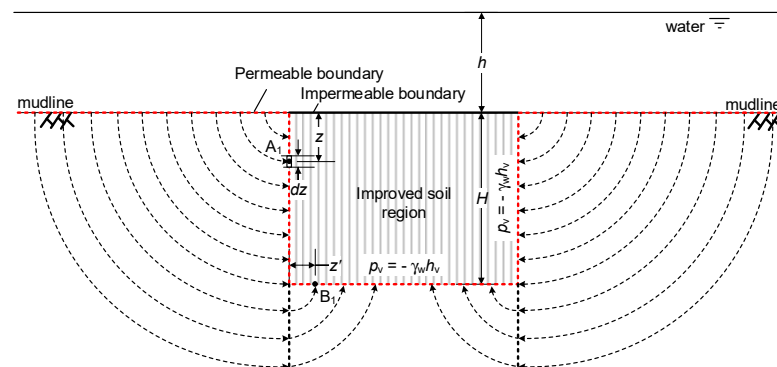


Figure 12. Illustration of proposed simplified flow paths under suction-induced seepage.

For seepage flow along the lateral boundary, a line element with a dimension  $dz$  at the depth of  $z$  was considered here (see Figure 12), the head loss  $\Delta h$  at the line element under the stable seepage can be written as

$$\Delta h = \frac{P_v}{\gamma_w} = h_v, \tag{16}$$

where,  $P_v$  is the vacuum pressure along the PVDs.

The corresponding hydraulic gradient,  $i_1(z)$  is expressed as

$$i_1(z) = \frac{2h_v}{\pi z}, \tag{17}$$

In accordance with Darcy’s law, the flow rate along the lateral boundary  $q_l$  is

$$q_l = 2k \int_{H_0}^H i_1(z) dz = \frac{4kh_v}{\pi} \ln\left(\frac{H}{H_0}\right), \tag{18}$$

where  $H_0$  is the penetration depth of the sealing membrane.

Regarding the seepage flow of the bottom boundary, the corresponding hydraulic gradient  $i_b$  at  $z'$  is

$$i_b(z') = \frac{2h_v}{\pi(H + 2z')}, \tag{19}$$

Similarly, the flow rate along the bottom boundary  $q_b$  is

$$q_b = 2k \int_H^{1.5H} i_b(z') dz' = \frac{2kh_v}{\pi} \cdot \ln \frac{4}{3}, \tag{20}$$

Combining Equations (18) and (20) gives the total seepage flow rate  $q$

$$q = \beta_1 q_l + \beta_b q_b = \frac{2kh_v}{\pi} \left[ 2\beta_1 \ln\left(\frac{H}{H_0}\right) + \beta_b \ln \frac{4}{3} \right], \tag{21}$$

where, two coefficients of  $\beta_1$  and  $\beta_b$  are introduced here for the further modification of reference seepage flow rate, aiming to capture a reasonable region of occurring seepage with varying  $B/H$ .

The correlation between  $\beta_1$ ,  $\beta_b$ , and  $B/H$  can be obtained by the back-calculation based on the FE results of operative seepage discharge of both lateral and bottom boundaries under different  $B/H$ , and can be expressed as

$$\beta_1 = 0.02 \frac{B}{H} + 1.9, \tag{22}$$

$$\beta_b = 21.2 - 20.5(0.6)^{B/H}, \tag{23}$$

It can be seen from Equation (21), the normalized operative seepage discharge  $Q/BH$  increased linearly with time when  $B/H$  and  $-h_v/H$  are known, and can be expressed

$$Q/BH = \frac{qt}{BH} = \frac{2kh_v}{\pi BH} \left[ 2\beta_1 \ln\left(\frac{H}{H_0}\right) + \beta_b \ln \frac{4}{3} \right], \tag{24}$$

Figure 13 shows the comparison of seepage discharges computed by Equations (21)–(23) obtained from FE analyses in scheme II. The total seepage discharge  $Q/BH$  are included for comparison with different  $B/H$  and  $-h_v/H$ . The reasonable prediction can be observed in general, with some deviations mainly in the earlier seepage, which was due to the assumption of stable-state flow.

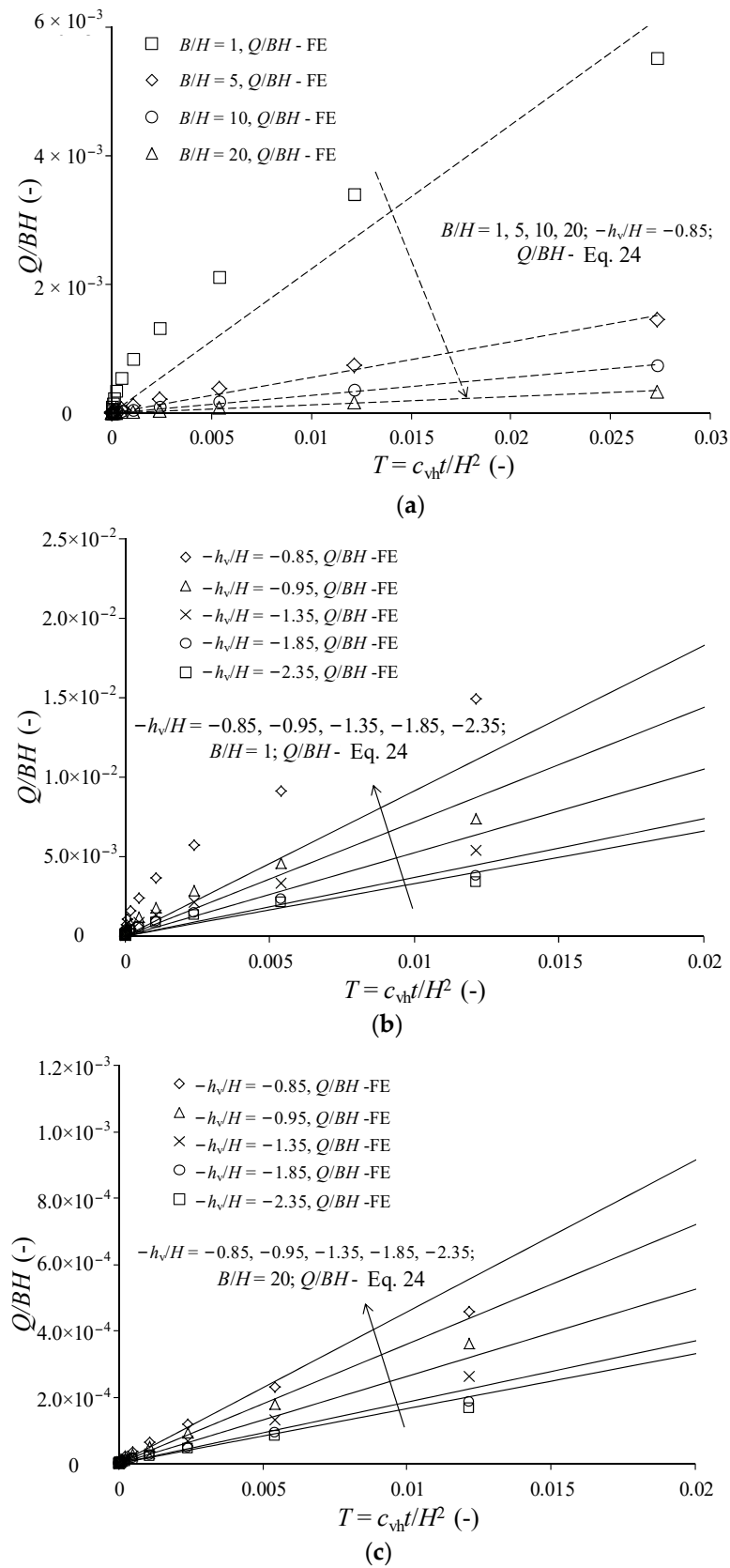


**Figure 13.** Comparison of the operative seepage discharges between the numerical and calculated results: (a) varied  $B/H$ ; (b)  $-h_v/H, B/H = 1$ ; (c)  $-h_v/H, B/H = 20$ .

### 4.3. Prediction of the Non-Uniform Settlement

Considering a negative contribution (“negative” settlement) of seepage to the settlement, the non-uniform settlement along the top surface of improved soil region with time was calculated in this section.

Retrospecting Equation (15), the central point settlement with different  $B/H$  under varying consolidation degrees  $(1 - U_s)$ , was first calculated as

$$S_i = (S_{\max} - S_{n,f})(1 - U_s), \tag{25}$$

where  $S_{n,f}$  is the final “negative” settlement induced by the seepage.

As discussed before,  $S_{n,f}$  was taken as 0 under  $B/H = 20$ , since the seepage influence can be neglected. For different  $B/H$ ,  $S_{n,f}$  was expressed as a function of normalized operative seepage discharge

$$S_{n,f} = \frac{Q}{B} \alpha_{n,f} = \frac{Q(T_c)}{B} \left( 5 - 0.2 \frac{B}{H} \right), \tag{26}$$

where  $\alpha_{n,f}$  is a modification coefficient to consider the influence of  $B/H$  on the negative settlement,  $T_c$  is the effective acting time factor of the seepage flow from the overlapping water.

For practical consideration, the vacuum stopped when the consolidation of the improved soil was completed, so  $T_c$  was calculated using Equation (6) (with  $S_{i1}$  reaching the maximum, and  $U_{s1} = 0$ )

$$T_c = \frac{c_{vh}t_c}{H^2} = \frac{36c_{vh}D_eF(n)}{9.9c_vD_e^2F(n) + 32c_hH^2}, \tag{27}$$

Substituting Equations (26) and (27) into Equation (25) yields the time-dependent settlement response at the central point along the top surface of improved soil region

$$S_i = \left[ S_1 - \frac{q}{B} \left( 5 - 0.2 \frac{B}{H} \right) \frac{36D_eF(n)H^2}{9.9c_vD_e^2F(n) + 32c_hH^2} \right] (1 - U_s), \tag{28}$$

The results computed by Equation (28) are shown in Figure 14, and compared with those from FE analyses in scheme III. The excellent agreement can be observed suggesting that Equation (28) was reasonable to estimate the settlement response of central point considering the influence of seepage flow.

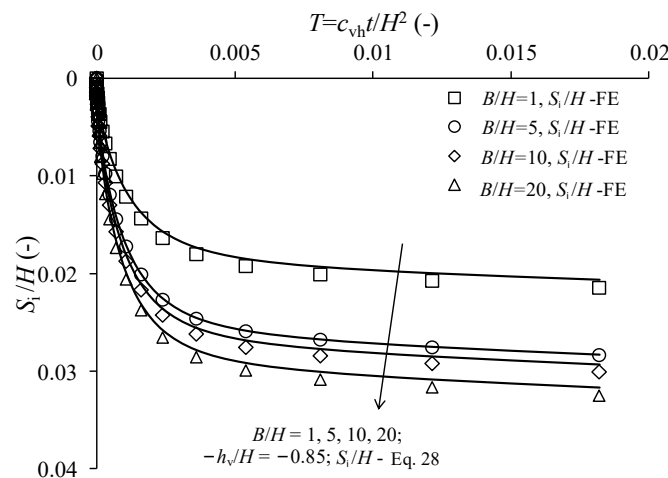


Figure 14. Comparison of time-dependent settlement responses at the central point between the numerical and calculated results.

Regarding the settlements for the positions away from the central point in the improved soil region  $S_{x/B}$ , its expression can be deduced based on Equation (28)

$$S_{x/B} = S_i \left\{ 1 - \left[ 1.3 + \left( 0.14 \frac{B}{H} \right)^{3.5} \right] \left( \frac{x}{B} \right)^{3+0.014 \left( \frac{B}{H} \right)^{1.9}} \right\}, \tag{29}$$

Figure 15 reports the normalized non-uniform settlement  $S_{x/B}/H$  calculated by Equation (29) for  $B/H = 20$  under different consolidation degrees ( $1 - U_s$ ). From the comparison of the corresponding results from FE analyses in scheme III, good agreement can be found, so the proof of validity for Equation (29) was confirmed.

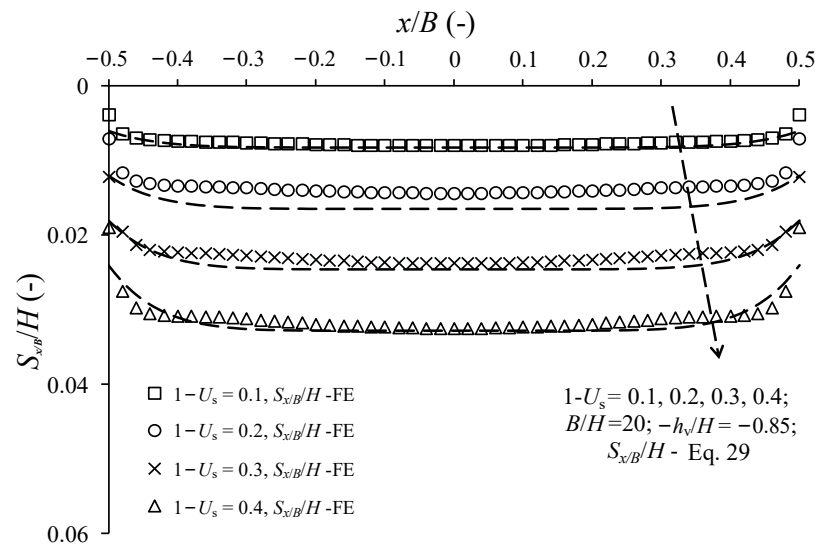


Figure 15. Comparison of time-dependent settlement responses at the central point between the numerical and calculated results.

### 5. Discussion

It was considered that the duration of the applied vacuum was generally 3 to 6 months with the very large  $B/H$  for the improved soil region in practice, referring to the application of onshore vacuum preloading with PVDs. This section therefore discusses the settlement responses under  $B/H = 20$  considering different water depth in the underwater vacuum preloading with PVDs, attempting to provide some implications and suggestions for engineering design.

Figure 16 reports the historical settlement for the central point at the top surface of improved soil under  $B/H = 20$  using the model of scheme III. The response of  $-h_v/H = -0.85$  could be thought as a reference without the contribution from the overlapping water, as the typical suction pressure of  $-85$  kPa similar to onshore vacuum preloading was applied and the influence of seepage was limited for the settlement of central point. By comparison with the settlement responses under different  $-h_v/H$ , if a duration of 6 months was taken for the vacuum application, larger settlement can be captured when the depth of overlapping water was higher. It means higher soil strength and better treatment would be available. In other words, a target settlement can be achieved in a shorter time. For instance, a settlement of  $0.03H$  required a duration of around 6 months in the onshore vacuum preloading (referring to the result of  $-h_v/H = -0.85$ ), but this time could be significantly reduced to 17 days when the improved soil was located in the water with depth of 10 m (referring to the result of  $-h_v/H = -1.85$ , assuming no loss in suction head).

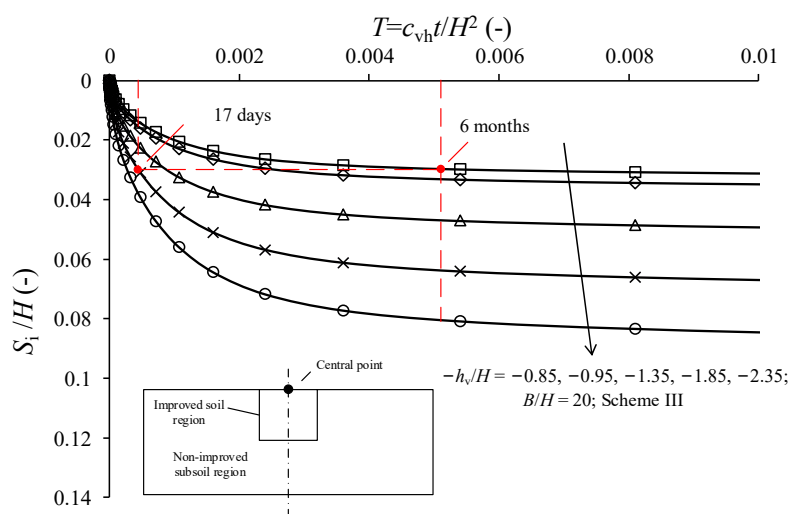


Figure 16. Comparison of time-dependent settlement responses at the central point under different water depths.

Figure 17 presents the non-uniform settlements along the top surface of improved soil region under different  $-h_v/H$ . For reference case of  $-h_v/H = -0.85$ , its response may not be thought to be similar to onshore vacuum preloading, although the non-uniform settlement also existed. Since the water–air mixture from lateral non-improved soil region flows into the improved soil region (especially for both sides), rather than continuous water in underwater vacuum preloading. Compared with other cases, the degree of non-uniform settlement increased as the water depth increased. It implied that the overlapping water could be used by submerged pump to increase the consolidation pressure, but meanwhile led to a significant non-uniform settlement.

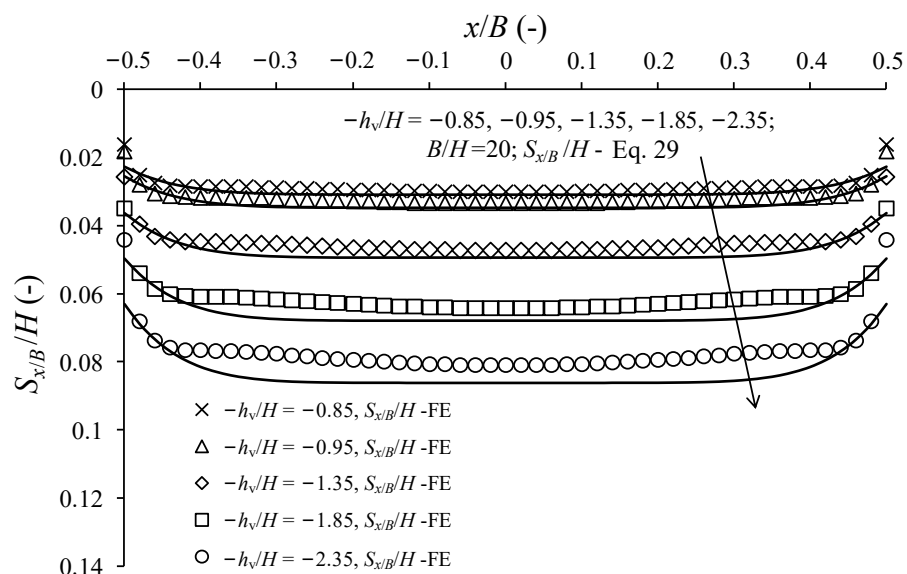


Figure 17. Comparison of time-dependent non-uniform settlement responses under different water depths.

### 6. Conclusions

This paper presented the comprehensive numerical investigation of settlement response in the underwater vacuum preloading with PVDs. The influential mechanism of overlapping water was examined and interpreted by comparison of soil behavior using

numerical analyses under suction-induced consolidation, seepage, and their combination. The main findings can be included as below.

- The overlapping water can be utilized as effective consolidation pressure (i.e., increasing the suction head) to improve the effect of soil treatment, or reduce the time of treatment, when the submerged pump was used in the underwater vacuum preloading with PVDs (perhaps relevant installation technologies required to be developed).
- The overlapping water can induce the significant non-uniform settlement along the top surface of improved soil region. It was different from onshore vacuum preloading with the water–air mixture rather than continuous water through both lateral and part of bottom boundary. This could be solved by the application of different suctions within the improved region, such as lower suction in the center and higher on both sides of the improved soil region.
- The dimension of improved soil region can influence the consolidation rate, with a faster rate as increasing  $B/H$ . Hence, a relatively larger  $B/H$  (i.e.,  $B/H \geq 5$ ) is recommended in practice.
- The higher vacuum pressure than onshore can be readily achieved once the water depth is sufficiently large, yet non-uniform settlement of seabed is more serious, and larger capacity of submerged pump (leading to high cost) is required. Hence, a proper vacuum pressure needs to be identified early by the proposed method in this paper.

Moreover, the proposed theoretical approach can be used to predict the time-dependent settlement response in the underwater vacuum preloading, yet further research is required to consider more influences, such as soil plasticity, smear effect, well resistance, and etc. However, it has to be recognized, this paper provided some fundamental understandings of underwater vacuum preloading, and also a general framework to estimate the settlement response with the influence of overlapping water.

**Author Contributions:** Conceptualization, S.L. and D.F.; methodology, S.L.; software, Y.Y.; validation, Z.Z. and Y.Y.; formal analysis, S.L.; investigation, S.L. and D.F.; resources, D.F. and S.Y.; data curation, D.F.; writing—original draft preparation, S.L. and D.F.; writing—review and editing, Y.Y. and Z.Z.; visualization, D.F.; supervision, S.Y.; project administration, S.Y.; funding acquisition, D.F., S.L. All authors have read and agreed to the published version of the manuscript.

**Funding:** This research was funded by National Natural Science Foundation of China, grant number 41877214 and the Scientific Research Foundation of Hainan University No. KYQD(ZR)20006.

**Institutional Review Board Statement:** Not applicable.

**Informed Consent Statement:** Not applicable.

**Acknowledgments:** The authors would like to acknowledge the support received from the National Natural Science Foundation of China No. 41877214 and the Scientific Research Foundation of Hainan University No. KYQD(ZR)20006.

**Conflicts of Interest:** The authors declare no conflict of interest.

## References

1. Yan, S.W.; Chu, J. Soil improvement for a storage yard using the combined vacuum and fill. *Can. Geotech. J.* **2005**, *42*, 1094–1104. [[CrossRef](#)]
2. Voottipruex, P.; Bergado, D.T.; Lam, L.G.; Hino, T. Backanalyses of flow parameters of PVD improved soft Bangkok clay with and without vacuum preloading from settlement data and numerical simulations. *Geotext. Geomembr.* **2014**, *42*, 457–467. [[CrossRef](#)]
3. Indraratna, B.; Zhong, R.; Fox, P.J.; Rujikiatkamjorn, C. Large-strain vacuum-assisted consolidation with non-darcian radial flow incorporating varying permeability and compressibility. *J. Geotech. Geoenviron. Eng.* **2017**, *143*, 04016088. [[CrossRef](#)]
4. Liu, R.; Yan, S.; Miao, Z.; Liu, A.; Zhang, J.; Guo, S.; Sun, W. Study of mechanism of vacuumization in underwater vacuum preloading. *China Harb. Eng.* **2003**, *05*, 29–43.
5. Feng, Y.Q.; Zhang, L. The application of vacuum preloading method in soft soil foundation underwater. *Appl. Mech. Mater.* **2014**, *580–583*, 209–212. [[CrossRef](#)]
6. Liu, Y. Application and Study of Underwater Vacuum Preloading Method. Master's Thesis, Tianjin University, Tianjin, China, 2015.

7. Chu, J.; Guo, W. Land reclamation using clay slurry or in deep water: Challenges and solutions. *Jpn. Geotech. Soc. Spec. Publ.* **2016**, *2*, 1790–1793. [[CrossRef](#)]
8. Karlsrud, K.; Gregersen, O.; Nerland, Ø.; Sparrevik, P.L. Vacuum consolidation of seabed clay—A full scale experiment. In Proceedings of the 14th European Conference on Soil Mechanics and Geotechnical Engineering, Madrid, Spain, 23–28 September 2007.
9. Tavenas, F.; Jean, P.; Leroueil, S. The permeability of natural soft clays, Part 2: Permeability characteristics. *Can. Geotech. J.* **1983**, *20*, 645–660. [[CrossRef](#)]
10. Shogaki, T.; Moro, H.; Masaharu, M.; Kaneko, M.; Kogure, K.; Sudho, T. Effect of sample disturbance on consolidation parameters of anisotropic clays. In *Proceedings of the Compression and Consolidation of Clayey Soils, Hiroshima, Japan, 10–12 May 1995*; A. A. Balkema: Rotterdam, The Netherlands, 1995; Volume 1, pp. 561–566.
11. Indraratna, B.; Redana, I.W. Laboratory determination of smear zone due to vertical drain installation. *J. Geotech. Eng. ASCE* **1998**, *124*, 180–184. [[CrossRef](#)]
12. Barron, R.A. Consolidation of fine grained soils by drain wells. *Trans. ASCE* **1948**, *113*, 324–360.
13. Hansbo, S. Consolidation of clay by band-shaped prefabricated drains. *Ground Eng.* **1979**, *12*, 16–25.
14. Bergado, D.T.; Asakami, H.; Alfaro, M.C.; Balasubramaniam, A.S. Smear effects of vertical drains on soft Bangkok clay. *J. Geotech. Eng. ASCE* **1991**, *117*, 1509–1530. [[CrossRef](#)]
15. Jamiolkowski, M.; Lancellotta, R. Consolidation by vertical drains—Uncertainties involved in prediction of settlement rates. Panel Discussion. In Proceedings of the 10th International Conference on Soil Mechanics and Foundation Engineering, Stockholm, Sweden, 15–19 June 1981; Volume 1, pp. 345–351.
16. Onoue, A.; Ting, N.H.; Germaine, J.T.; Whitman, R.V. Permeability of disturbed zone around vertical drains. In Proceedings of the Geotechnical Engineering Congress, Boulder, CO, USA, 10–12 June 1991; pp. 879–890.
17. Jamiolkowski, M.; Lancellotta, R.; Wolski, W. Precompression and speeding up consolidation. General Report: Special Session 6. In Proceedings of the 8th European Conference on Soil Mechanics and Foundation Engineering, Helsinki, Finland, 23–26 May 1983; Volume 3, pp. 1201–1226.
18. Rixner, J.J.; Kraemer, S.R.; Smith, A.D. Prefabricated Vertical Drains. In *Summary of Research Report-Final Report*; Report No. FHWA-RD-86/169; Federal Highway Administration: Washington, DC, USA, 1986; Volume I–III, p. 433.
19. Holtz, R.D.; Jamiolkowski, M.; Lancellotta, R.; Pedroni, S. Prefabricated vertical drains: Design and performance. In *CIRIA Ground Engineering Report: Ground Improvement*; Butterworth-Heinemann Ltd.: Oxford, UK, 1991; p. 131.
20. Hird, C.C.; Pyrah, I.C.; Russell, D.; Cinicioglu, F. Modeling the effect of vertical drains in two-dimensional finite element analyses of embankments on soft ground. *Can. Geotech. J.* **1995**, *32*, 795–807. [[CrossRef](#)]
21. Chai, J.C.; Miura, N.; Sakajo, S.; Bergado, D. Behavior of vertical drain improved subsoil under embankment loading. *J. Soil Found.* **1995**, *35*, 49–61. [[CrossRef](#)]
22. Hansbo, S. Consolidation of fine-grained soils by prefabricated drains. In Proceedings of the 10th International Conference on Soil Mechanics and Foundation Engineering, Stockholm, Sweden, 15–19 June 1981; Volume 3, pp. 677–682.
23. Indraratna, B.; Redana, I.W. Closure: Plane strain modeling of smear effects associated with vertical drains. *J. Geotech. Geoenviron. Eng. ASCE* **1999**, *125*, 96–99. [[CrossRef](#)]
24. Indraratna, B.; Redana, I.W. Plane strain modeling of smear effects associated with vertical drains. *J. Geotech. Eng. ASCE* **1997**, *123*, 474–478. [[CrossRef](#)]
25. Hu, L. Consolidation behavior of soft soil subjected to on-land and underwater vacuum preloading. Ph.D. Thesis, The Hong Kong University of Science and Technology, Hongkong, China, 2010.
26. Zhang, J.; Liu, A. Analysis of mechanism of consolidation of soil improved with underwater vacuum preloading method. *Chin. J. Geotech. Eng.* **2007**, *29*, 644–649.
27. Liu, A. Influence of varied water pressure loading on strengthening effect of vacuum preloading. *China Earthq. Eng. J.* **2015**, *2*, 467–471.
28. Lee, N. Analytical, centrifuge and numerical modelling of underwater vacuum consolidation of soft clay. Ph.D. Thesis, The Hong Kong University of Science and Technology, Hongkong, China, 2007.
29. Wang, C. Study of Mechanism of Underwater Vacuum Preloading. Master's Thesis, Tianjin University, Tianjin, China, 2005.
30. Dassault Systèmes. *Abaqus Analysis User's Manual*; Simulia Corp: Providence, RI, USA, 2010.
31. Bergado, D.; Balasubramaniam, A.; Fannin, R.; Holtz, R. Prefabricated vertical drains (pvds) in soft bangkok clay: A case study of the new bangkok international airport project. *Can. Geotech. J.* **2002**, *39*, 304–315. [[CrossRef](#)]
32. Mesri, G.; Khan, A. Ground Improvement Using Vacuum Loading Together with Vertical Drains. *ASCE J. Geotech. Geoenviron. Eng.* **2012**, *138*, 680–689. [[CrossRef](#)]
33. Chu, J.; Yan, S. *Application of the Vacuum Preloading Method in Soil Improvement Projects*; Geo-Engineering Book Series; Elsevier: Amsterdam, The Netherlands, 2005.
34. Hu, L.; Wang, Y.; Liu, Z. Centrifuge modelling on soft soil subjected to underwater vacuum preloading. *Proc. Inst. Civ. Eng. Ground Improv.* **2019**, *172*, 167–178. [[CrossRef](#)]
35. Indraratna, B.; Rujikiatkamjorn, C.; Kelly, R. Modeling of combined vacuum and surcharge preloading with vertical drains. In Proceedings of the 17th International Conference on Soil Mechanics and Geotechnical Engineering, Alexandria, Egypt, 5–9 October 2009; pp. 2204–2207.

36. Rujikiatkamjorn, C.; Indraratna, B.; Chu, J. 2D and 3D numerical modeling of combined surcharge and vacuum preloading with vertical drains. *Int. J. Geomech.* **2008**, *8*, 144–156. [[CrossRef](#)]
37. Ye, G.; Xu, Y.; Zhang, Z. Performance evaluation of pvd-reinforced soft soil with surcharge and vacuum preloading. *Int. J. Civil. Eng. Trans. A Civil. Eng.* **2018**, *16*, 421–433. [[CrossRef](#)]
38. Al-Tabbaa, A. Permeability and Stress-Strain Response of Speswhite Kaolin. Ph.D. Thesis, University of Cambridge, London, UK, 1987.
39. Gourvenec, S.; Randolph, M.F. Consolidation beneath circular skirted foundations. *Int. J. Geomech.* **2010**, *10*, 22–29. [[CrossRef](#)]
40. Fox, P.J.; Berles, J.D. A piecewise-linear model for large strain consolidation. *Int. J. Numer. Anal. Methods Geomech.* **1997**, *21*, 453–575. [[CrossRef](#)]
41. Schiffmann, R.L.; Chen, A.T.F.; Jordan, J. An analysis of consolidation theories. *J. Soil Mech. Found. Div.* **1969**, *95*, 285–313. [[CrossRef](#)]
42. Booker, J.R.; Small, J.C. The behaviour of an impermeable flexible raft on a deep layer of consolidating soil. *Int. J. Numer. Analyt. Meth. Geomech.* **1986**, *10*, 311–327. [[CrossRef](#)]
43. Gourvenec, S.; White, D. Elastic solutions for consolidation around seabed pipelines. In Proceedings of the Annual Offshore Technology Conference, Houston, TX, USA, 3–6 May 2010; Volume 2, pp. 996–1010.
44. Yeung, A.; So, S.; Kwong, A.; Tham, L.; Zhao, W. Field-scale constructability evaluation of underwater vacuum preloading. *Geomech. Geoengin. An. Int. J.* **2009**, *4*, 245–252. [[CrossRef](#)]
45. Vermeer, P.A.; Verruijt, A. An accuracy condition for consolidation by finite elements. *Int. J. Numer. Analyt. Meth. Geomech.* **1981**, *1*, 1–14. [[CrossRef](#)]
46. Carrillo, N. Simple two- and three-dimensional cases in the theory of consolidation of soils. *Stud. Appl. Math.* **1942**, *21*, 1–5. [[CrossRef](#)]
47. Terzaghi, K. *Erdbaumechanik auf Bodenphysikalischer Grundlage*; Franz Deuticke: Leipzig, Germany, 1925; p. 399.